to chlorine atoms on adjacent molecules), while the closest U–Cl distance (from uranium to chlorine atoms on the same molecule) would remain unchanged, again as observed.

Diffraction data can only tell us the average structure of this material, but all four observed changes in this average structure (strong vibration of Cl perpendicular to the UCl bond, expansion of the c axis, vibration of the entire molecule along c, and constancy of the U–Cl bond lengths within a molecule) strongly suggest that the phase transition observed by DEA can only involve the onset of hindered rotation of UCl₄ molecules about their unique z axis.

Many examples of such phase transitions involving hindered rotations are known, the most famous examples being the ammonium halides, where the NH₄ tetrahedra commence rotation even at low temperature. Levy, Sanger, Taylor & Wilson (1975) have found similar hindered rotations commencing at high temperature in halide octahedra such as MoF₆, and no doubt many others will be found when structural measurements close to the melting point become more common. Such dynamic disorder, though strongly suggested by the present elastic diffraction measurements, could only be proved using inelastic scattering techniques.

Apart from offering an explanation for a phase transition in this class of materials, we have also demonstrated that such compounds form essentially simple molecular structures made from UX_4 units. In fact, these UCl₄ units probably remain intact even in the liquid phase. This simple molecular picture contrasts with the more complex coordinations previously suggested for uranium in such compounds.

Finally, at the other extreme, we might have expected that at least one more phase transition would lower the symmetry at low temperature. The volume of the structure could be reduced by a static co-related tilting of the tetrahedra, with the chlorine atoms moving toward the z-axis channels, and such cooperative static rotations of tetrahedra are well known (*e.g.* in BiVO₄; David, Glazer & Hewat, 1979). However, in the case of UCl₄ the structure remains tetragonal down to the lowest temperatures.

References

BOGACZ, A., BROS, J. P., GAUNE-ESCARD, M., HEWAT, A. W. & TAYLOR, J. C. (1980). *J. Phys. C*, **13**, 5273–5278.
BOGACZ, A., SZCZEPANIAK, W., BROS, J. P., FOUQUE, Y. & GAUNE-ESCARD, M. (1984). *J. Chem. Soc. Faraday Trans.* 1, **80**, 2935–2941.
BROS, J. P., FOUQUE, Y., GAUNE-ESCARD, M., SZCZEPANIAK, W. & BOGACZ, A. (1982). *J. Chim. Phys.* **79**, 715–718.
DAVID, W. I. F., GLAZER, A. M. & HEWAT, A. W. (1979). *Phase Transitions*, 1, 155–170.
FOUQUE, Y., BROS, J. P., GAUNE-ESCARD, M., SZCZEPANIAK, W. & BOGACZ, A. (1980). *J. Inorg. Nucl. Chem.* **42**, 257.
FOUQUE, Y., GAUNE-ESCARD, M., SZCZEPANIAK, W. & BOGACZ, A. (1978). *J. Chim. Phys.* **75**, 360.
HEWAT, A. W. (1973). *J. Phys. C*, **6**, 2559–2572.
HEWAT, A. W. (1979). *Acta Cryst.* A35, 248.
HEWAT, A. W. & BAILEY, I. (1976). *Nucl. Instrum. Methods*, **137**, 463–471.
HEWAT, A. W., TAYLOR, J. C., GAUNE-ESCARD, M., BROS, J. P., SZCZEPANIAK, W. & BOGACZ, A. (1984). *J. Phys. C*, **17**, 4587–4600.
JOHNSON, C. K. (1965). *ORTEP*. Report ORNL-3794. Oak Ridge National Laboratory, Tennessee.
KHAN MALEK, CH., DELAMOYE, P., HUSSONNOIS, M. & GUIBÉ, L. (1980). *10 ème Journées des Actinides*, 27–28 May, Stockholm.
LEVY, J. H., SANGER, P. L., TAYLOR, J. C. & WILSON, P. W. (1975). *Acta Cryst.* B31, 1065–1067.
MOONEY, R. C. L. (1949). *Acta Cryst.* 2, 189–191.
MUCKER, K., SMITH, G. S., JOHNSON, Q. & ELSON, R. (1969). *Acta Cryst.* B25, 2362–2365.
MULAK, J. & ZOLNIEREK, Z. (1976). *Proceedings of the 2nd International Conference on the Electronic Structure of the Actinides*, Wroclaw, Poland, 13–16 September.
PASCAL, P. (1960). *Nouveau Traité de Chimie Minérale*, Vol. XV, p. 144. Paris: Masson.
RIETVELD, H. M. (1969). *J. Appl. Cryst.* 2, 65–71.
TAYLOR, J. C. & WILSON, P. W. (1973). *Acta Cryst.* B29, 1942–1944.
YOSHIMURA, T., MIYAKE, C. & IMOTO, S. (1971). *J. Nucl. Sci. Technol.* pp. 498–502.

The Incommensurate Structure of Mullite by Patterson Synthesis

BY R. J. ANGEL* AND C. T. PREWITT*

Department of Earth and Space Sciences, State University of New York, Stony Brook, NY 11794-2100, USA

Abstract

The incommensurate structure of a mullite, Al₂[Al$_{2+2x}$, Si$_{2-2x}$]O$_{10-x}$, with $x = 0.40$, has been solved by the analysis of Patterson functions constructed from satellite intensity data collected by single-crystal X-ray diffractometry. The analysis shows that the incommensurate modulation is comprised of two sets of ordering patterns (difference structures) which have different symmetries, and which are modulated in quadrature through the crystal. One difference

* Present address: The Geophysical Laboratory, Carnegie Institution of Washington, 2801 Upton St. NW, Washington, DC 20008, USA.

structure belongs to the Shubnikov space group $P_c nnm$, and is shown to order O atoms and vacancies on the bridging oxygen site, Oc, of the double tetrahedral chains of mullite. There is also an associated ordering of overall site occupancy between the two tetrahedral sites within the structure. The second difference structure has symmetry $P_c bnm$, and orders aluminium and silicon between the two tetrahedral sites. The small displacements of the O atoms associated with tetrahedral site ordering have also been defined. The extreme stability of the mullite structure is shown to be due to its employing two ordering schemes, both of which resemble ordering patterns found in the related stoichiometric structures, sillimanite and ι-alumina. In addition, it is shown that these two ordering patterns fit together in such a way as to allow the incommensurate mullite structure to employ both ordering schemes simultaneously in approximately one-third of the crystal volume.

Introduction

Mullite is an aluminosilicate refractory with composition $Al_2[Al_{2+2x}Si_{2-2x}]O_{10-x}$, with the compositional variable x ranging (in principle) from zero to unity. When $x = 0$ the structure is that of (disordered) sillimanite, Al_2SiO_5, while at $x = 1$ it resembles the structure proposed for the iota polymorph of alumina, Al_2O_3. This range of composition is based upon the exchange $2Si^{4+} + O^{2-} = 2Al^{3+} + \square$, where $\square$ represents an oxygen vacancy. The structure of mullite can therefore be thought of as being derived from that of disordered sillimanite by the removal of oxygen anions and the exchange of aluminium for silicon (e.g. Angel & Prewitt, 1986). In order to accommodate this compositional variation, mullite develops an incommensurate structure whose periodicity varies continuously with composition.

The average structure of mullite consists of chains of edge-sharing AlO_6 octahedra which run parallel to the c axis. Parallel to these are double chains of Al/Si tetrahedra, denoted T (Fig. 1). The oxygen anions removed from the structure come from the Oc site which provides the central cross link of the double chains. Removal of such an O atom reduces to threefold the coordination of the two adjacent tetrahedral (T) sites. Such a configuration is unstable, and the cations are transferred from these positions to adjacent, more distorted, T^* sites (Fig. 1). This transfer of tetrahedral cations is accompanied by displacements of the coordinating oxygen anions as indicated in Fig. 1. This pattern of tetrahedral and Oc site occupancies represents the average structure of mullite and has been determined in several structure refinements (Sadanaga, Tokonami & Takeuchi, 1962; Burnham, 1964; Durovic, 1969; Durovic & Fejdi, 1976). More recently, Angel & Prewitt (1986) used high-order tensor coefficients in a refinement to identify the displacements of the Oab and Od atoms associated with the transfer of cations between the T and T^* sites.

In addition to the Bragg reflections from which the average structure is determined, diffraction patterns of mullites contain a number of additional diffraction maxima (Agrell & Smith, 1960). The most intense of these are pairs of satellites disposed around the positions of Bragg reflections which arise from ordering in sillimanite, but which are absent from mullite (Fig. 2). The presence of such satellites around $l =$ half-integer positions in diffraction patterns from mullite indicates that some form of ordering is developed within the mullite structure which doubles the c axis to that of sillimanite, and which has a long and incommensurate periodicity along the a axis.
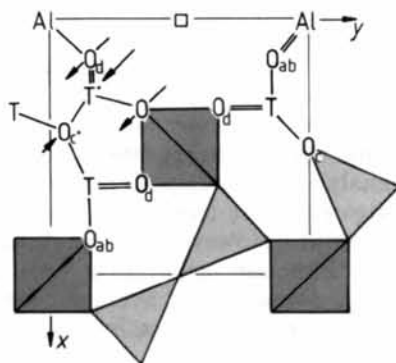

Fig. 1. The derivation of the average structure of mullite from sillimanite. Operation of the exchange $2Si^{4+} + O^{2-} \rightarrow 2Al^{3+}$ requires the formation of oxygen vacancies on the Oc sites. The formation of one such vacancy at, for example, $x = 0$, $y = \frac{1}{2}$ leads to the transfer of the adjacent tetrahedral cations to T^* sites, accompanied by the displacements of O atoms indicated by arrows.
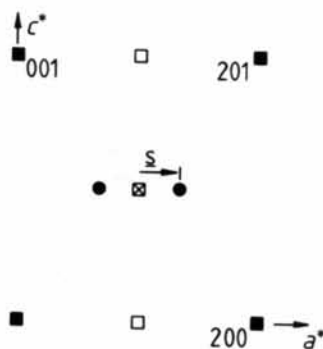
Fig. 2. a^*–c^* reciprocal-lattice section of mullite, for which $h =$ odd reflections are absent (open squares). The crossed square represents the position of the ordering reflections in sillimanite, but which are absent from mullite. The filled circles indicate the positions of the satellites observed in mullite. Cameron (1977a) showed that their wavevector, s, lies parallel to a^* for compositions $0.2 < x < 0.5$, and that its modulus varies linearly with composition in this range.

In this paper we describe a new analysis of these satellite reflections which represents the first full application of various techniques recently developed by McConnell & Heine (1984, 1985b) for the analysis of incommensurate structures. In particular, the precise symmetry analysis of the incommensurate modulation (McConnell & Heine, 1984) is used to interpret various Patterson functions (McConnell & Heine, 1984) and projections (McConnell & Heine, 1985b) calculated from satellite intensities alone. These are 'difference Pattersons' (Freuh, 1953; Takeuchi, 1972), and are related to differences between the ordering schemes and the average structure of the material. Unlike previous methods used to analyse satellite data, these Patterson functions require no prior assumptions in their interpretation. The fact that we have achieved a complete and self-consistent structural analysis (apart from a little uncertainty over Al/Si distributions due to their similar X-ray scattering factors) indicates the power of these methods. We should emphasize that the symmetry analysis carried out by McConnell & Heine (1984, 1985b) is quite independent of the mechanism proposed by Heine & McConnell (1984) for the origin of incommensurate structures in insulators, and thus the validity of the analytical methods employed here is not dependent upon the mechanism responsible for the incommensurate modulation in mullite. However, we do believe that mullite is a good example of this particular mechanism, in that the analysis shows that the incommensurate structure arises from the modulation in quadrature (that is displaced by a phase of $\pm 90°$, or a distance of $\lambda/4$, along the modulation wave) of *two* ordering schemes with different symmetries.

We shall demonstrate that the first ordering scheme, or difference structure, orders oxygens and vacancies on the Oc sites. Coupled with this is an ordering of tetrahedral site occupancies (Al plus Si) between the T and T^* sites, such that a vacancy on an Oc site gives rise to the transfer of a cation (Al or Si) from the 'normal' tetrahedral site T to the 'alternative' site T^*. This is essentially the same ordering scheme as seen in the average structure, and generates a structure which resembles that of the iota polymorph of alumina.

The second component structure closely resembles that of sillimanite. Ordering of oxygens and vacancies is not permitted by the symmetry and, as a consequence, the overall occupancies of the tetrahedral sites remain approximately the same as those of the average structure. The Patterson functions do show evidence of ordering of Al and Si on the sillimanite pattern, accompanied by small displacements of all of the O atoms. Taken together these displacements are equivalent to rotation of the AlO_6 octahedra. Precisely the same distortions are present in the structure of sillimanite.

The exceptional stability of the mullite structure therefore derives, in part, from the presence of both of these ordering schemes within the structure. Examination of the way in which these ordering patterns are distributed within the crystal shows that they are able to co-exist simultaneously in approximately one-third of the crystal volume. It is this overlap which is the source of the interaction between the ordering schemes which stabilizes the incommensurate structure of mullite.

Previous models

Various models have been proposed for the ordering in mullite. Those based upon high-resolution transmission electron microscope (HRTEM) studies (Nakajima & Ribbe, 1981; Yla-Jaaski & Nissen, 1983) favour antiphase domain or block structures, with the oxygen vacancies concentrated on the antiphase domain boundaries (a.p.b.'s). The incommensurate repeat corresponding to the satellite spacings arises from the average spacing of the a.p.b.'s not being a commensurate multiple of the average structure. However, HRTEM imaging studies suffer from the strong interaction of electrons with crystalline specimens which leads to much stronger double diffraction effects in the electron microscope than occur for X-ray diffraction. These can often generate diffracted beams that appear to correspond to higher-order satellites. The inclusion of such beams in the formation of an image inevitably leads to the 'squaring up' of the high-resolution image of a modulated structure, so that it appears to consist of domains. Although some squaring up of the modulation might be expected in mullite, neither of the models proposed in these two studies is capable of accommodating the compositional range $0 < x < 0.5$. They do however provide possible models for high-alumina mullites ($x > 0.5$) in which the wave vector of the modulation is not parallel to a^*. Such structures are beyond the scope of the current paper.

By contrast, X-ray diffraction avoids, for the most part, problems of double diffraction. It has one further advantage over TEM; the intensity data from the satellites and from the Bragg reflections can be collected and analysed separately, so that the ordering can be investigated apart from contributions from the average structure. However, the one disadvantage of an X-ray diffraction experiment is that it only provides a time-and-space average over the entire specimen, rather than direct information on local environments.

Tokonami, Nakajima & Morimoto (1980) investigated satellite and diffuse intensity from a mullite of composition $x = 0.372$. They suggested that oxygen/vacancy ordering results in the clustering of vacancies in an incommensurate structure which they modelled with a large supercell. In principle, the

analysis of satellite intensity on the basis of a supercell should result in a structure identical to that produced by Patterson analysis. However, as Tokonami, Nakajima & Morimoto (1980) pointed out, conventional refinement methods are unable to distinguish between many different supercell models because of the very similar R values which result.

Saalfeld (1979) also suggested that the oxygen vacancies formed clusters, but within a smaller, $10a \times b \times 2c$, supercell. His model, based upon an optical transform of satellite intensity data, includes some features similar to those that result from our Patterson analysis. Saalfeld's model includes two types of tetrahedral double chains; one like those found in sillimanite, and the other arising from the removal of alternate Oc bridging oxygens along the c axis. In our model all of the chains have a proportion of Oc oxygens removed, the proportion varying from chain to chain. However, the arrangement of the two types of chains in Saalfeld's model is such that there is no periodicity within the structure which corresponds to the observed spacing of satellites in mullite diffraction patterns. In fact, structure-factor calculations show that Saalfeld's (1979) $10a$ supercell model generates greater diffraction intensities at $\pm\frac{2}{3}|s|$ than at $\pm|s|$. Such intensity has not been reported for any mullite.

The results of this study differ from the models previously proposed for mullite in four major respects. Most significantly, it is shown that not one but two distinct ordering patterns are present within the mullite structure. Secondly, the redistribution of aluminium and silicon between the two tetrahedral sites is shown to be a major component of the ordering schemes. Thirdly, the oxygen vacancies are *not* clustered, but are distributed throughout the structure. Finally, the distortions of the oxygen packing which accompany the ordering on the tetrahedral sites are identified for the first time.

Experimental

The mullite crystal used for this study was the same as that whose average structure was reported by Angel & Prewitt (1986). It was previously described as sample no. 5 by Cameron (1977a,b), and has a composition corresponding to $x = 0.40$, with trace amounts of iron. Cell parameters are given by Angel & Prewitt (1986). Single-crystal X-ray precession photographs of several fragments of this sample all showed moderately sharp satellite reflections around $l = \frac{1}{2}$ positions of the average structure (Fig. 2). The satellite vector s (Fig. 2) was parallel to a*, and had a magnitude of $0.30a*$.

Intensity data from the satellite reflections were collected on a Picker four-circle diffractometer with ω-2θ scans in a constant precision mode ($\sigma_I/I < 0.01$, maximum count time 300 s) and with graphite-monochromatized Mo $K\alpha$ radiation ($\lambda = 0.7107$ Å).

Satellites in one octant of reciprocal space were collected out to $2\theta = 90°$, using as a standard reflection the 362 Bragg peak. A second data collection out to $2\theta = 110°$ of all the satellite pairs around $0kl$ Bragg positions was also carried out, in order to provide a check on the symmetry analysis of mullite of McConnell & Heine (1985a). The raw data were corrected for Lorentz and polarization effects, but no corrections were made for absorption [μ(Mo $K\alpha$) = 10.7 cm^{-1}] or extinction. The presence of satellites around positions in the diffraction pattern of the average structure which have half-integer values of l indicates that the unit cell of the ordered structure has a doubled c axis of 5.77 Å. Each satellite pair was indexed on this doubled cell so that they only occur for odd values of l.

The Patterson maps used in this study were calculated using programs written around the Cambridge Crystallography Subroutine Library (CCSL, Matthewman, Thompson & Brown, 1982). In order to calculate the plus and minus Pattersons (McConnell & Heine, 1984, 1985b), the satellite intensities are shifted to the Bragg position central to each pair. Such a shift should be accompanied by a correction to the intensities to allow for the variation of scattering factors with $\sin \theta/\lambda$ (*e.g.* Cochran, 1968). Such a correction was not made as it requires a knowledge of the distribution of scatterers giving rise to the satellite intensities. However, calculation indicated that, in the worst possible case, such corrections would amount to less than 7% of the structure factor (5% of the intensity), and in most cases are less than 2%.

Analysis of component structures

Heine & McConnell (1984) showed that, on the basis of Landau theory, an incommensurate structure could develop from an ordering transition in insulators providing certain symmetry requirements are fulfilled. The most important of these is that there must exist two ordering schemes which have the symmetries of a pair of irreducible representations of the space group of the disordered structure. Heine & McConnell (1984) proposed that it is the interactions between these two ordering schemes that stabilize the incommensurate phase, and that this interaction is maximized by having them modulated in quadrature. They therefore write the scattering density in the crystal (McConnell & Heine, 1984) as

$$\rho(\mathbf{r}) = \rho_{ave}(\mathbf{r}) + \rho_1(\mathbf{r}) \cos \mathbf{q} \cdot \mathbf{r} + \rho_2(\mathbf{r}) \sin \mathbf{q} \cdot \mathbf{r} \quad (1)$$

where $\rho_{ave}(\mathbf{r})$ is the scattering density of the average structure, and $\rho_1(\mathbf{r})$, $\rho_2(\mathbf{r})$ are the differences of the two ordering schemes from the average structure. These difference structures therefore contain regions of positive and negative scattering density, much as the difference structures derived from ordering

reflections in commensurately ordered structures such as simple alloys (Fig. 3). These are modulated in quadrature by the sine and cosine terms in which q is the wave vector of the modulation. The actual structure therefore consists of planar regions, normal to the wave vector, in which the structure is $\rho_{ave}(r) + \rho_1(r)$ followed by $\rho_{ave}(r) + \rho_2(r)$, then $\rho_{ave}(r) - \rho_1(r)$ etc. Between such regions are areas in which both ordering schemes are present. It is clear that when such a 'boundary' region approximates the structure of both pure components then the incommensurate phase is further stabilized. This can therefore be seen as the source of the interaction between the ordering schemes which stabilizes a modulated structure (Heine & McConnell, 1984; McConnell & Heine, 1985a).

Such a formulation of the scattering density leads to the Bragg reflections in the diffraction pattern of a modulated structure being dependent upon the scattering density distribution, $\rho_{ave}(r)$, of the average structure alone. It also results in a diffraction pattern in which only first-order satellite reflections appear. The amplitudes of these depend only upon the difference densities $\rho_1(r)$, $\rho_2(r)$, and are independent of the distribution of atoms in the average structure.

Structural analysis of such materials can therefore proceed by two separate stages. The intensities of the Bragg reflections can be used to refine the average structure in a conventional manner. However, care must be taken, as the average structure contains information about atom displacements in the form of closely spaced 'split-atom' sites. The intensity of the satellites cannot be processed in such a straightforward manner, as the amplitude of a pair of satellites is given by (McConnell & Heine, 1984)

$$A(g \pm q) = \tfrac{1}{2}A_1(g \pm q) \pm \tfrac{1}{2}iA_2(g \pm q), \qquad (2)$$

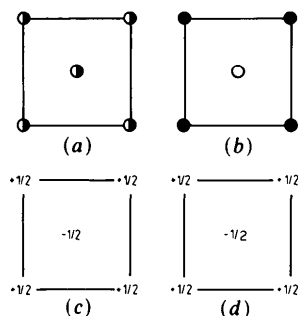where $A(g \pm q)$ are the amplitudes of the two satellites

Fig. 3. Ordering in a simple AB structure. In the average structure (a) each site is statistically occupied by $0.5A + 0.5B$. (b) On ordering of the atoms two sites may be distinguished by their occupancies. The difference structure (c) is simply the difference between the ordered and disordered states. The weights represent the magnitude of the difference from the average structure in units of A atoms (filled circles). The difference Patterson map (d) is the Patterson map of the difference structure in (c).

at $\pm q$ from the Bragg position g, and $A_i(g \pm q)$ are the structure factors arising from the difference structure $\rho_i(r)$. Each individual satellite therefore contains contributions from both difference structures, unless there is a systematic absence for one component at g. In order to refine the difference structures $\rho_1(r)$ and $\rho_2(r)$ it is necessary to deconvolute the data present in the satellites. This requires prior knowledge of the difference structures, and the refinement process must proceed by a process of iteration in which trial difference structures are used in the deconvolution, and better trial structures are found by refinement to the deconvoluted data.

Such a process is a 'direct method'. The alternative is to use the 'indirect' method of Patterson synthesis. McConnell & Heine (1984) showed that there are two Patterson functions which may be formed from the satellite intensities, and which may be interpreted in terms of $\rho_1(r)$ and $\rho_2(r)$. These are termed the 'plus' and 'minus' difference Patterson functions, and are constructed by respectively adding and subtracting each pair of satellite intensities at the Bragg position central to each pair. The plus Patterson function is then the sum of the Pattersons of $\rho_1(r)$ and $\rho_2(r)$, while the minus Patterson function is a cross-correlation function:

$$P_+(R) \propto \int \rho_1(r)\rho_1(r+R) + \rho_2(r)\rho_2(r+R) \, d^3r$$
$$P_-(R) \propto \int \rho_1(r)\rho_2(r+R) - \rho_2(r)\rho_1(r+R) \, d^3r. \qquad (3)$$

Because the symmetries of $\rho_1(r)$ and $\rho_2(r)$ are one-dimensional irreducible representations of a space group (Heine & McConnell, 1984), they are isomorphic with black/white or Shubnikov groups (Indenbom, 1960). In addition to containing normal symmetry operators (even functions), the Shubnikov groups also contain operators which are odd functions (i.e. change sign). The latter relate areas of equal positive and negative difference density in the difference structures $\rho_1(r)$ and $\rho_2(r)$. Consequently the corresponding plus and minus Patterson functions contain vector density of both positive and negative weights, and possess the symmetries of Shubnikov groups. The patterns of weights in the plus and minus Patterson functions can therefore be used to identify the symmetries of the difference structures $\rho_1(r)$ and $\rho_2(r)$, much as conventional Patterson functions constrain the symmetries of conventional structures (McConnell & Heine, 1985b).

The formalism represented by (1) is strictly only applicable to structures just below the transition from the disordered to the incommensurate phase. However, in the absence of satellite reflections of higher than first order, there is no information on which to base more complex structural analyses. Such a case apertains in the current study of mullite, as single-crystal precession photographs did not exhibit second-order satellites.

Table 1. *Irreducible representations of mullite which allow ordering*

	$E\|000$	$C_{2x}\|\frac{1}{2}\frac{1}{2}0$	$m_y\|\frac{1}{2}\frac{1}{2}0$	$m_z\|000$	$E\|001$	$C_{2x}\|\frac{1}{2}\frac{1}{2}1$	$m_y\|\frac{1}{2}\frac{1}{2}1$	$m_z\|001$	$i\|000$	$m_x\|\frac{1}{2}\frac{1}{2}0$	$C_{2y}\|\frac{1}{2}\frac{1}{2}0$	$C_{2z}\|000$	$i\|001$	$m_x\|\frac{1}{2}\frac{1}{2}1$	$C_{2y}\|\frac{1}{2}\frac{1}{2}1$	$C_{2z}\|001$
X_1	1	1	1	1	-1	-1	-1	-1	1	1	1	1	-1	-1	-1	-1
X_2	1	1	1	1	-1	-1	-1	-1	-1	-1	-1	-1	1	1	1	1
X_7	1	-1	-1	1	-1	1	1	-1	1	-1	-1	1	-1	1	1	-1
X_8	1	-1	-1	1	-1	1	1	-1	-1	1	1	-1	1	-1	-1	1

Patterson functions

Symmetries

The hypothetical high-temperature disordered phase from which the incommensurately ordered mullite may be considered to be derived would have the symmetry of the average structure (*Pbam*). The possible symmetries of the difference structures were derived by McConnell & Heine (1985a) by consideration of the symmetry of the ordering vector, $\frac{1}{2}\mathbf{c}^* + |\mathbf{s}|\mathbf{a}^*$. The component along $\mathbf{c}^*$ represents a doubling of the c axis of the difference structures relàtive to that of the average structure. Of the four possible pairs of irreducible representations of *Pbam* which could correspond to the difference structures, only two pairs (Table 1) allow any ordering at all within the structure. These were designated X_1, X_2 and X_7, X_8 by McConnell & Heine (1985a). They may be distinguished by the signs of the vector density of self-peaks at $U = \frac{1}{2}$, $W = 0$ in the plus Patterson function as shown in Fig. 4. In the plus Patterson function calculated from the mullite satellites (Fig. 5) all of these self-peaks are negative (the peak at $V = 0.42$ is the combination of two peaks corresponding to T^*-T^* vectors with $U = 0.48$ and $U = 0.52$). The plus Patterson function therefore shows that the symmetries of

the difference structures giving rise to the incommensurate modulation in mullite have the symmetries of the pair of representations X_7, X_8. This was the conclusion reached by McConnell & Heine (1985a) on crystal-chemical grounds. The equivalent Shubnikov space groups are respectively W_{58}^{401}, P_cnnm, and P_cbnm which is a non-standard orientation of W_{62}^{451}, P_bnma.

These symmetries mean that the difference structure with P_cnnm symmetry (X_7) does not contribute to the satellite pairs around $0kl$ positions with k even, while that with P_cbnm symmetry (X_8) does not contribute to k odd reflections in $0kl$. Consideration of (2) shows that in such a case the intensities of the two members of each satellite pair should be equal. This was confirmed by a statistical test on the $0kl$ satellite pairs which showed that of 364 such pairs only 32 (9%) had amplitudes that differed by greater than one standard deviation calculated from counting statistics. Of these only two pairs were different by between 2σ and 3σ.

Patterson projections

Because the $0kl$ satellite pairs contain contributions from either one difference structure or the other, they may be split into two groups, of k even and k odd reflections, from which Patterson projections onto

Fig. 4. Identification of the irreducible representations corresponding to the ordering schemes in mullite. (*a*) The pattern of signs of symmetry-related sites (at $z = 0$) in difference structures with symmetries X_1, X_2 and X_7, X_8. The signs of the sites at $z = \frac{1}{2}$ are the reverse of those shown in all cases. (*b*) The difference Patterson maps corresponding to these ordering patterns. Only that of X_7, possibly with a contribution from X_8, can match the Patterson function calculated from the satellite intensities of mullite (*c*).

Fig. 5. A (001) section at $W = 0$ of the plus Patterson function of mullite. Both U and V axes run from 0 to 0.6; contours are at arbitrary levels, and are dashed for negative values. Peaks identified by a single label are 'self-peaks', arising from vectors between symmetry-related sites.

(100) may be calculated. These projections (Fig. 6) are separate projections of the two difference structures.

Because the X-ray scattering factors of aluminium and silicon are very similar, vectors in the Patterson functions arising from Al/Si ordering on tetrahedral sites will be very weak compared with vectors to sites on which the overall (Al *plus* Si) occupancies are changed. The Patterson projection of the $P_c nnm$ component (Fig. 6a) shows strong vectors involving both types of tetrahedral site, as well as vectors between these and the Oc and Oc^* positions. This difference structure therefore includes strong ordering of the overall occupancies of the tetrahedral sites, as well as oxygens and vacancies. By contrast, the Patterson projection of the $P_c bnm$ difference structure (Fig. 6b) is dominated by vectors to the Oc^* site, indicating that overall tetrahedral site occupancies are less ordered in this component than the displacements of the oxygens around the Oc position. The weaker vectors to the tetrahedral sites appear to arise from ordering of aluminium and silicon. The absence of vectors to Oc sites from Fig. 6(b) should also be noted. This is because the Oc site occupies symmetry centres at $\frac{1}{2}, 0, \frac{1}{2}$ (and equivalents) in the average structure, which become anticentres in $P_c bnm$. Ordering on the Oc site is therefore not allowed in this difference structure, and is restricted to that with $P_c nnm$ symmetry.

Both Patterson projections show significant vector density either side of the plane $W = \frac{1}{4}$, which can only arise from vectors to the Od sites at heights $z = \frac{1}{4}, \frac{3}{4}$ in the ordered (2c) unit cell. The pattern of positive and negative lobes in the vector density is characteristic of small displacements of one of the atoms giving rise to the vector (Takeuchi, 1972). In this case, the Od sites are displaced parallel to the c axis from $z = \frac{1}{4}$ in both components. These displacements were also

apparent in the high-resolution structure refinement of this same crystal (Angel & Prewitt, 1986).

The plus Patterson

The self peaks in the plus Patterson function (Fig. 5) constructed from the hkl satellite pairs have already been used to identify the symmetries of the difference structures. The remaining vector density in P_+ can now be interpreted in the light of information obtained from the Patterson projections. The latter show that tetrahedral site occupancy is far more strongly modulated by the $P_c nnm$ difference structure than that of $P_c bnm$ symmetry. All of the vectors involving the T and T^* sites which appear in the plus Patterson function can therefore be interpreted, to a first approximation, as arising from the $P_c nnm$ difference structure. For example, the peak at $U = 0.12$, $V = 0.13$, $W = 0$ (Fig. 5) is between adjacent T and T^* sites. Its negative weight indicates that all such pairs of sites in the $P_c nnm$ difference structure have opposite signs arising from the transfer of atoms from one site (negative difference density) to the other (positive difference density).

Analysis of the average structure (Angel & Prewitt, 1986) showed that the Oab oxygen site undergoes small displacements within the (001) plane depending upon which of the T or T^* sites is occupied. Several peaks in the plus Patterson function can be assigned to vectors involving the Oab sites. The signs of these show that the Oab atoms are displaced towards the occupied tetrahedral sites in the $P_c nnm$ difference structure. In $P_c bnm$ this oxygen site is always displaced towards those T^* sites that possess positive difference density.

The minus Patterson

Equation (3) shows that the minus Patterson function is a cross-correlation function between the two difference structures $\rho_1(\mathbf{r})$ and $\rho_2(\mathbf{r})$. When ordering occurs on the same set of sites in both difference structures, as it does in mullite, the P_- function provides further information on the ordering patterns. In particular, once the symmetries of the two components are known the minus Patterson function defines the relative phase of the two components. This is necessary because (1) contains a phase ambiguity in that the structure it describes is distinct from that generated by replacing $\rho_1(\mathbf{r})$ by $-\rho_1(\mathbf{r})$, or $\rho_2(\mathbf{r})$ by $-\rho_2(\mathbf{r})$. This would be equivalent to a relative phase change of π from a phase difference between $\rho_1(\mathbf{r})$ and $\rho_2(\mathbf{r})$ of $\pi/2$ to one of $-\pi/2$. In mullite the peaks at $U = \frac{1}{2} - 2x$, $V = \frac{1}{2}$, $W = 0$ in the minus Patterson function arise from the cross-correlation function between the same sets of sites in the two difference structures; they are 'self-peaks' whose weight and sign depend upon the signs of the difference densities of the same sites in the two ordering schemes. Fig. 7
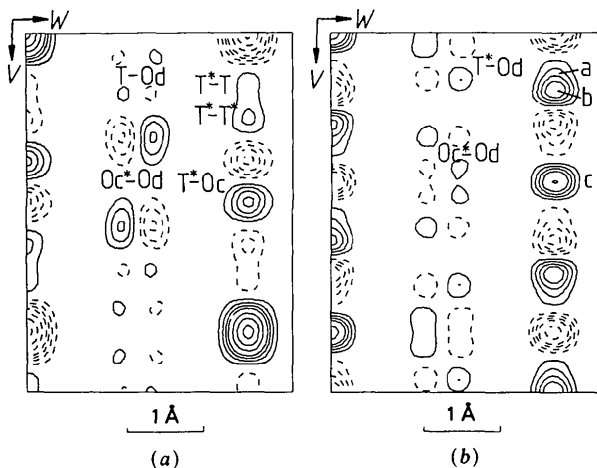

Fig. 6. Separate Patterson projections onto (100) of the two difference structures. (a) $P_c nnm$. (b) $P_c bnm$, peak a is due to T^*-T^* vectors, peak b to Oc^*-Oc^* vectors, and peak c to T^*-Oc^* and Od-Od vectors.

shows how the signs of these peaks are dependent upon the relative signs of the two ordering patterns on a given set of sites in the two difference structures.

Examination of the minus Patterson function (Fig. 8) allows the relative signs of the tetrahedral sites in the two ordering schemes to be defined. The peak at $U = 0.02$, $V = \frac{1}{2}$, $W = 0$ arises from the cross-correlation between T^* sites in the two difference structures, and its weight is positive. This indicates that the signs of the difference density of the T^* sites at $x = 0.24$, $y = 0.76$ are the same in both difference structures. By contrast, the T sites at $x = 0.15$, $y = 0.34$ must have opposite signs in the two difference structures because the peak in the minus Patterson function at $U = 0.2$, $V = \frac{1}{2}$, $W = 0$ is negative.

In mullite there is zero ordering on the Oc site in the P_cbnm difference structure for symmetry reasons. This is confirmed by the absence of any vector density at $U = \frac{1}{2}$, $V = \frac{1}{2}$, $W = 0$ in the minus Patterson function (Fig. 8). Since the overall tetrahedral site occupancies are seen to be correlated with the oxygen/vacancy distribution (cf. the average structure), the difference density on the tetrahedral sites in the P_cbnm ordering scheme must be due to Al/Si ordering. This is in contrast to the P_cnnm difference structure in which the difference density on the tetrahedral sites is dominated by the overall occupancy which masks the effect of any ordering of aluminium and silicon.

The vector density at $U = 0.40$, $V = \frac{1}{2}$, $W = 0$ in the minus Patterson function arises from the cross-correlation function between the Oc^* sites in the two difference structures. The positive sign of this peak indicates that the Oc^* sites at $x = 0.05$, $y = 0.55$ have the same sign in both difference structures, a result which can also be deduced from the Patterson projections (Fig. 6) together with the information on the relative signs of the tetrahedral sites provided by the minus Patterson function. The remaining peak at $V = \frac{1}{2}$ in the minus Patterson function appears to be due to a small displacement of the T site parallel to the a axis. Such a displacement would also account for the pair of peaks in the minus Patterson function around $U = \frac{1}{2}$, $V = 0.16$, $W = 0$. The peaks in the minus Patterson function at more general positions are identified in Fig. 8. Their signs are consistent with the relative signs of the ordering patterns deduced above.

Discussion

Analysis of the Patterson functions described above identifies the patterns of ordering within the two difference structures of mullite (Fig. 9). In some cases the relative weights of Patterson peaks give an indication of the relative magnitude of the ordering on various sites. However, the absolute amplitude of these ordering schemes is not defined; we do not know whether a particular site is as fully ordered as possible (maximally ordered), or whether it only attains a state of partial order. Calorimetric data on incommensurate 'e'-plagioclases (Carpenter, McConnell & Navrotsky, 1985) suggest that they attain the maximum possible state of order allowed by the constraints of the structure. In the absence of any evidence to the contrary we will therefore assume

Fig. 7. The deduction of the relative phases of $\rho_1(\mathbf{r})$ and $\rho_2(\mathbf{r})$ from the minus Patterson function. (a) The ordering pattern in P_cnnm for a given set of symmetry-related sites, together with the two possibilities in P_cbnm for the same set of sites. The minus Patterson function, P_-, arising from the combination of P_cnnm ordering pattern with the first of the possibilities with P_cbnm symmetry is shown in (b), that from the second in (c). Parts (i) and (ii) in (b) and (c) represent the respective contributions of $\rho_1(\mathbf{r})\rho_2(\mathbf{r}+\mathbf{R})$ and $\rho_2(\mathbf{r})\rho_1(\mathbf{r}+\mathbf{R})$ (equation 3) to the P_- function. Note that the sign of the horizontal ($U = \frac{1}{2} - 2x$, $V = \frac{1}{2}$, $W = 0$) and diagonal vectors differ in the two cases, and the signs of these peaks can be used to distinguish which of the two P_cbnm ordering schemes in (a) represents $\rho_2(\mathbf{r})$.
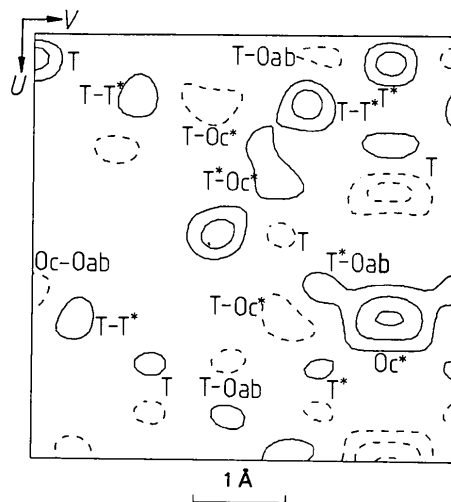

Fig. 8. A (001) section at $W = 0$ of the minus Patterson function of mullite over the same region of vector space, and scaled identically to the plus Patterson function of Fig. 5.

for the sake of discussion that the mullite crystal studied here is maximally ordered.

In incommensurate structures the occupancy of any given site is represented by $\rho(r) = \rho_{ave}(r) + \rho_1(r)\cos q \cdot r + \rho_2(r)\sin q \cdot r$ (equation 1). Every site within the crystal must have an occupancy given by $\rho(r)$ which is between zero and unity. Therefore, in order to calculate the maximum amplitudes of $\rho_1(r)$ and $\rho_2(r)$ permitted, the average occupancies of the sites within the crystal must also be known. These were determined for this mullite crystal by Angel & Prewitt (1986) and are listed in Table 2. The ranges of site occupancies given in Table 2 then represent the maximum allowed variation in this crystal. Analysis of the Patterson functions indicates that almost all of this variation occurs in the P_cnnm difference structure.

The resultant pure component structures, based upon the application of the principal of maximal ordering to mullite, are drawn in Fig. 10. They are the actual structure of the crystal on planes where the value of $q \cdot r$ (equation 1) is such that one or other of the difference structures does not contribute to $\rho(r)$. For example, where $q \cdot r = 2n\pi$ (n integral), $\sin q \cdot r$ is zero, and the structure consists of $\rho_{ave}(r) + \rho_1(r)$. It is in these pure component structures, and in the difference structures which generate them, that the crystal-chemical basis for the stability of mullite is to be found.

As described in the *Introduction*, the major feature of the P_cnnm difference structure is the ordering of oxygens and vacancies on the Oc sites. It should be noted that it is the *overall* occupancy by O atoms of the region around this site that is ordered (*i.e.* Oc plus $2Oc^*$). The small displacements from the symmetry centre of ~ 0.5 Å, represented by the Oc^* sites,

Table 2. *Site occupancies*

	Average†		P_cnnm Amplitude	Range
T	0·81 (3)	0·8	+0·2	0·6–1·0
T^*	0·19 (3)	0·2	−0·2	0·4–0·0
$Oc+2Oc^*$	0·77 (3)	0·8	+0·2	0·6–1·0
Oc	0·39 (1)	0·4	+0·1	0·3–0·5
Oc^*	0·19 (1)	0·2	+0·05	0·15–0·25

† Average site occupancies from Angel & Prewitt (1986) are given in the first column and rounded off in the second. The latter correspond to values in Fig. 10.

are a secondary effect. Coupled to this oxygen/vacancy ordering is a transfer of atoms between adjacent T and T^* sites, as indicated by their opposite signs in the difference structure (Fig. 9a). Application of the principle of maximal ordering (Table 2) generates a pure component structure which has two types of tetrahedral environment (Fig. 10a).

In one half of this pure component the T site is fully occupied and T^* is completely vacant, while in the other half a transfer of atoms from T to T^* doubles the occupancy of T^* relative to the average structure. For the reasons discussed above it is not possible to derive directly from the Pattersons the

(a)

(b)
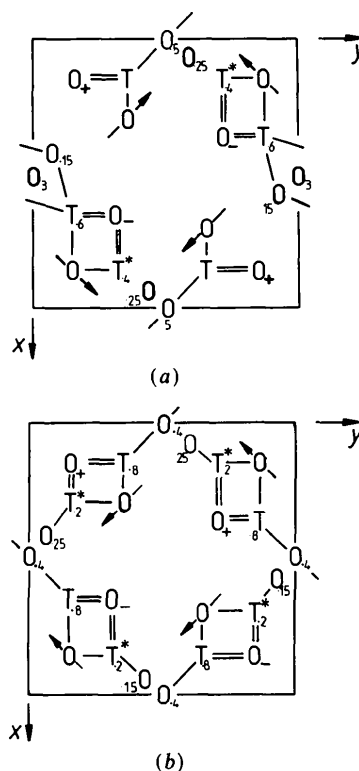
Fig. 10. Sections at $z = \frac{1}{2}$ of the pure component structures derived from applying the principle of maximal ordering to the difference ordering patterns of Fig. 9 and the average structure determined by Angel & Prewitt (1986). Site occupancies are given only for partially occupied sites. Arrows indicate displacements of Oab sites, $+/-$ the upward/downward displacement of Od sites at $z = \frac{1}{4}$. (a) P_cnnm, (b) P_cbnm.
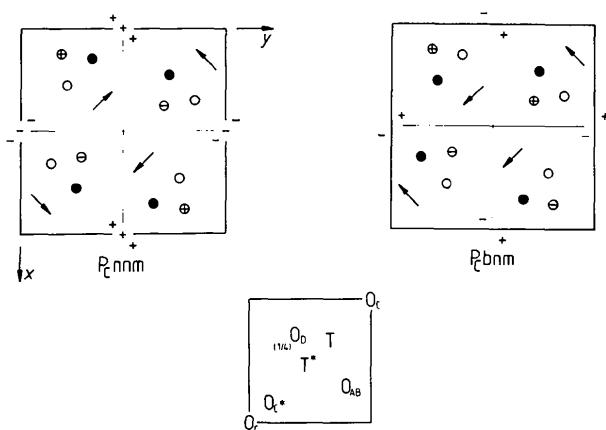

Fig. 9. The patterns of difference density in sections at $z = \frac{1}{2}$ for the two ordering schemes. ●/○ = positive/negative density on tetrahedral sites; $+/-$ = positive/negative density on Oc and Oc^* sites. Arrows indicate the direction of displacement of Oab oxygens, and ⊕/⊖ the displacements (up/down) of the Od sites at $z = \frac{1}{4}$. The key below identifies the sites in the upper left quadrant of each difference structure.

distribution of aluminium and silicon in this component. However, the displacements of the coordinating atoms may be used to infer differences in the Si:Al ratio between tetrahedral sites. Bonds between Si and O tend to be shorter than Al–O linkages in the same environment, so that movement of O atoms towards a tetrahedral site may indicate an increase in its Si:Al ratio in the component structure over that in the average structure. Care must be taken not to confuse this effect with that seen, for example, for the Oab site in the P_cnnm difference structure, which always moves towards the tetrahedral site whose occupancy is increased relative to the average structure.

The movements of the Od atoms are always towards the more occupied T sites, and away from the more occupied T^* sites, in the P_cnnm difference structure (Fig. 9a). The fact that this movement is also towards the more occupied Oc sites and away from vacancies suggests that it is caused by T–Od bonding requirements over and above Oc–Od repulsion. This shortening of T–Od bonds suggests that the T sites adjacent to occupied Oc sites are enriched in silicon relative to the average structure. The coupled increase in the length of the bond between the Od atom and the more occupied T^* site in the adjacent layer suggests in turn that the latter site is enriched in aluminium.

The third oxygen site in the structure is Oc, which is the central bridging atom of the tetrahedral double chains. The Oc^* site has often been interpreted in the average structure as a displacement imposed upon the Oc oxygen by the occupation of an adjacent T^* tetrahedral site. If this were the case then the occupancy of the Oc^* site in the pure P_cnnm component would be equal to that of the adjacent T^* sites. However, when the average occupancies are taken into account, this would result in the occupancies of adjacent Oc and Oc^* sites being ordered in antiphase. This is in contradiction to the evidence from the Patterson functions which constrains the signs of these two sites in the P_cnnm difference structure to be the same (Fig. 9a). The occupancies assigned to these sites in the pure component structure (Fig. 10a) satisfy this condition, but may well be of incorrect magnitude. Even so, it may be deduced that the displacement of the Oc oxygen off the symmetry point is not dependent exclusively upon the occupancy or otherwise of the adjacent T^* site, but probably also depends upon the species in both that site and the two T sites bonded to it.

The P_cbnm component structure is not allowed by symmetry to order oxygens and vacancies on the Oc site. There is therefore no need for the ordering scheme to vary the overall occupancy of the tetrahedral sites. The difference density at the tetrahedral sites in the P_cbnm difference structure (Fig. 9b) has therefore been interpreted as arising from Al/Si

ordering, with positive difference density representing an increase in the Si:Al ratio of a site relative to that found in the average structure. The displacements associated with all three oxygen sites support his intepretation. The Oab site moves towards Si-enriched tetrahedral sites, while the Od site is displaced towards Si-enriched T^* sites at the expense of lengthening the bonds to Si-enriched T sites. The displacement of the bridging oxygen of the tetrahedral double chains, represented by the occupancy pattern of the Oc^* site, is also away from Al-enriched T sites and towards Si-enriched ones. This is similar to the pattern of displacements of the bridging oxygen in sillimanite (which does not have any T^* sites), but its different direction indicates that in this component the primary influence on the displacement of the Oc oxygen is the species occupying the T^* site.

It is interesting to note that the pattern of movements of the Oab and Od sites associated with the P_cbnm component structure is exactly that seen in sillimanite with decreasing temperature (Winter & Ghose, 1979). So not only does the P_cbnm component order aluminium and silicon on the sillimanite scheme, but the structural distortions also parallel those of the sillimanite structure. Unfortunately, the structure of ι-alumina, which may well resemble that of the P_cnnm component, has yet to be refined. No doubt similar parallels between this component and its corresponding end-member structure will become obvious once this work is carried out.

Heine & McConnell (1984) have shown how, in general terms, the stabilization energy of an incommensurate structure can arise from it employing two ordering schemes. In brief, because of the difference in symmetry between these two ordering schemes their interaction has to be of the gradient type. This means that the interaction occurs where the amplitude of one ordering scheme is decreasing and the other is increasing. That is, at the 'boundary' where one ordering scheme is giving way to the other, the two overlap. In the case of mullite, the two ordering schemes fit together in such a way that the last atomic plane of one is identical to the first atomic plane of the next, $i.e.$ the two patterns overlap on that plane. This is shown in Fig. 11 for a complete cycle of $\mathbf{q}\cdot\mathbf{r}$ from zero to 2π for a value of $|\mathbf{q}|$ equal to $\frac{1}{3}|\mathbf{a}^*|$. Note that the sequence $\rho_1, \rho_2, -\rho_1, -\rho_2, \ldots$ (and not $\rho_1, -\rho_2, -\rho_1, \rho_2, \ldots$) is uniquely determined by the minus Patterson function. The figure indicates why mullite is so stable. Fully one third of the crystal volume satisfies both ordering schemes simultaneously. This large region of overlap between the pure component structures is the source of the interaction which makes mullite such a stable refractory material.

This study has therefore identified the main aspects of the two ordering schemes in mullite, has confirmed the symmetry analysis of McConnell & Heine

(1985a), and has demonstrated the power of the analytical methods developed by McConnell & Heine (1984, 1985b). However, some work remains to be done. The amplitudes of the ordering schemes cannot be reliably determined from the Patterson functions, and must be obtained by direct refinement of the component structures. Secondly, the Al/Si ordering pattern proposed here for the $P_c nnm$ difference structure was deduced from the pattern of oxygen displacements. Such a deduction needs to be confirmed by neutron diffraction studies which will be capable of distinguishing directly between Si and Al atoms.
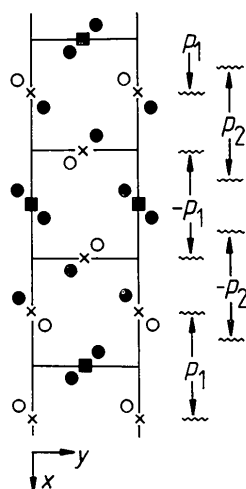
Fig. 11. The pattern of difference density in a mullite with a modulation vector of about $\frac{1}{3}a^*$. Only T sites ($\bullet$/O = Si/Al) and $Oc - Oc^*$ oxygen sites ($\blacksquare$/× = occupied/disordered) are shown. The regions of overlap between $\rho_1(r)$, $\rho_2(r)$ etc., where both ordering patterns are satisfied are indicated. Note that all the 'boundaries' between the pure components exhibit overlap, and therefore stabilize the modulation.

References

AGRELL, S. O. & SMITH, J. V. (1960). J. Am. Ceram. Soc. 43, 69–76.
ANGEL, R. J. & PREWITT, C. T. (1986). Am. Mineral. 71, 1476–1482.
BURNHAM, C. W. (1964). Carnegie Inst. Washington Yearb. 63, 223–228.
CAMERON, W. E. (1977a). Am. Mineral. 62, 747–755.
CAMERON, W. E. (1977b). Am. Ceram. Soc. Bull. 56, 1003–1007.
CARPENTER, M. A., MCCONNELL, J. D. C. & NAVROTSKY, A. (1985). Geochim. Cosmochim. Acta, 49, 947–966.
COCHRAN, W. E. (1968). Inelastic Neutron Scattering, Vol. 1, pp. 275–280. Vienna: International Atomic Energy Agency.
DUROVIC, S. (1969). Chem. Zvesti, 23, 113–128.
DUROVIC, S. & FEJDI, P. (1976). Silikaty, 20, 97–112.
FREUH, A. J. (1953). Acta Cryst. 6, 454–456.
HEINE, V. & MCCONNELL, J. D. C. (1984). J. Phys. C, 17, 1199–1220.
INDENBOM, V. L. (1960). Sov. Phys. Crystallogr. 4, 578–580.
MCCONNELL, J. D. C. & HEINE, V. (1984). Acta Cryst. A40, 473–482.
MCCONNELL, J. D. C. & HEINE, V. (1985a). Phys. Rev. B, 31, 6140–6142.
MCCONNELL, J. D. C. & HEINE, V. (1985b). Acta Cryst. A41, 382–386.
MATTHEWMAN, J. C., THOMPSON, P. & BROWN, P. J. (1982). J. Appl. Cryst. 15, 167–173.
NAKAJIMA, Y. & RIBBE, P. H. (1981). Am. Mineral. 66, 142–147.
SAALFELD, H. (1979). Neues Jahrb. Mineral. Abh. 134, 305–316.
SADANAGA, R., TOKONAMI, M. & TAKEUCHI, Y. (1962). Acta Cryst. 15, 65–68.
TAKEUCHI, Y. (1972). Z. Kristallogr. 135, 120–136.
TOKONAMI, M., NAKAJIMA, Y. & MORIMOTO, N. (1980). Acta Cryst. A36, 270–276.
WINTER, J. K. & GHOSE, S. (1979). Am. Mineral. 64, 573–586.
YLA-JASAKI, J. & NISSEN, H.-U. (1983). Phys. Chem. Mineral. 10, 47–54.